

# Calculation of Optical Constants of $\text{As}_{40}\text{S}_{60-x}\text{Se}_x$ Thick Films with High Accuracy using Wedge Shape Optical Model

A. Almohammed<sup>\*</sup>

Physics Department, Faculty of Science, Islamic University, P. O. Box 170, Al Madinah, Saudi Arabia

Received: 23 Oct. 2021, Revised: 12 Dec. 2021, Accepted: 20 Jan. 2022

Published online: 1 May 2022

**Abstract:** This work has been focused primarily on the extraction of thicknesses, optical, and AC electrical parameters for as-prepared  $\text{As}_{40}\text{S}_{60-x}\text{Se}_x$  thin films, with ( $x=0, 20, 40,$  and  $60$  at. %). The thickness of such films has been calculated by the wedge method depending on the transmission spectra of their shrinkage in the range of  $400$  to  $2500$  nm. Swanepoel's wedge relationships have been solved using the Mathcad 2000 program by *minerr* function to extract the film's thickness. Depending on the obtained thickness of studied the thin films, the main optical parameters have been determined. The structural aspects of the studied thin films have also been studied using XRD and SEM techniques.

**Keywords:**  $\text{As}_{40}\text{S}_{60-x}\text{Se}_x$  thin films; Wedge-shaped model; thin films; Optical constants; Energy gap.

## 1 Introduction

Chalcogenide glass is a surprising optical material due to its high linearity and nonlinear refractive index. Therefore, they represent a key element of continued technological progress in the field of optoelectronics and magnetic devices. Also, for these reasons, they have been used in many scientific and daily applications, and they are described as the mother of modern technology, or more precisely, the backbone of technological development [1].

Thus, these materials are widely utilized in semiconductor devices, the fields of telecommunications, spacecraft, medical and military systems, paint and heating tools, solar and photovoltaic systems, computer chips, smart windows, optical emitting diodes, optical conductors, and electromagnetic/ magneto-optic memories [1, 2], etc. All these applications are attributed to their smaller phonon energies as compared to the other oxide glasses [3] and their better-infrared transmission [4, 5]. Many efforts have been done to develop the mathematical formulation describing both the transmittance and the reflectance of different optical systems [6–13]. An investigation on chalcogenide thin films in the binary and ternary system of As-S-Se is suitable for utilizing in optical devices and the interest in such glasses has been previously discussed [14, 15].

Based on what has been mentioned, the precise identification of constants and optical parameters is very important, and this importance is not limited to understanding the basic mechanisms caused by all these effects, but also extends to the use of these materials in modern technology. As to the method utilizes to determine the optical constants and parameters of thin films that linked to it, one must consider that, in case of the optical thickness of the thin film is enough to create sundry interference extremes, it is possible to compute both of the refractive index and extinction coefficient or what called the optical constants from the transmission spectrum alone [7, 11, 16–22]. Other efforts also contributed extremely to updating, characterizing, and summarizing the overall thermal and optical properties where most of these efforts were focused on describing optical systems via the transmittance spectrum alone [7, 8, 11, 23–29]. We also had a great interest and effort in studying the optical, thermal, and electrical properties of As-S-Se alloys and their thin films fabricated by thermal evaporation [30–32].

In the current framework, we will mainly use the analysis of Swanepoel [7] to extract the thickness of as-prepared studied thin films. The aforementioned analysis is based on the possibility of converting non-uniform thickness transmittance into uniform thickness spectroscopy in a manner that approximates the typical description where it is applied to computed the average

<sup>\*</sup>Corresponding author E-mail: arda@iu.edu.sa

thickness, thickness changes, and refractive index from the main transmission spectrum of a wedge-shaped for as-deposited thin films in the mentioned range. In this present framework, we will concentrate fundamentally on all these properties, which are surely those that demand a much more itemized computation method in the present explanation which are the most rarely found in the literature. After extracting the thickness of the studied films, we will discuss in detail the optical parameters and their relationship to the different selenium content for thin films of similar thickness. Finally, we will study the electrical properties and we will discuss the dielectric constants ( $\epsilon'$ ,  $\epsilon''$ ), dissipation factor  $\tan \delta$ , dielectric modules ( $M'$ ,  $M''$ ) and the AC conductivity,  $\sigma_{AC}$  of the studied compositions and discussing the electrical parameters and constants linked to AC conductivity.

## 2 Experimental Methods

High purity powder (99.999 %) from Aldrich Company for the elements in the studied comositins was used to prepare the  $As_{40}S_{60-x}Se_x$  thin films, where ( $x=0, 20, 40$  and  $60$  at. %) onto ultrasonically cleaned glass substrate kept at 373 K via a thermal evaporation unit (Denton Vacuum DV 502 A) under a vacuum of  $10^{-6}$  Pa. Both the film thickness and the deposition rate were controlled using a quartz crystal monitor DTM 100. The deposition rate was kept at 2 nm/s during the preparation of thin films. The structure of the thin films were examined by X-ray diffraction (XRD) (Philips X-ray diffractometry (1710)) with Ni-filtered  $CuK_{\alpha}$  radiation with ( $\lambda = 0.15418$  nm). Both the morphology the elemental compositions of the As-S-Se thin films were analyzed by an energy dispersive X-ray spectrometer unit (EDXS) interfaced with a scanning electron microscope, SEM (JOEL XL) operating an accelerating voltage of 30 kV. The relative error of determining the indicated elements did not exceed 2 %. The measurements of the transmittance,  $T$  was carried out in terms of a double-beam spectrophotometer (Jasco V670) at normal incidence of light in a wavelength ( $\lambda$ ) range between 400 and 2500 nm. The measured transmittance spectrum was carried out without a glass substrate in the reference beam to calculate the refractive index and the film thickness of As-S-Se thin films according to Swanepoel's method. Using the RCL Bridge (Stanford Research Model: SR-720), the measuring device was calibrated at a frequency value equal to 1 kHz and in the thermal range between 298 to 793 K. Electrodes were made on the substrate upon which the thin film was deposited, by coating the substrate with a smooth layer of silver paste so that the substrate was divided into two halves separated by a shadow. So that the film becomes after painting as if it were a capacitor. The temperature of the films was carried out utilizing a Chromel–Alumel type K thermocouple located as close as possible to the thin films.

## 3 Theoretical Backgrounds

In terms of the Swanepoel relationship, the transmission of thin films of uniform thickness,  $d$  and their complex refractive index,  $\tilde{n}$  which equaled to  $\tilde{n} = n - ik$  and  $\alpha$  refers to an absorption coefficient can be expressed as follows [7, 17]:

$$T(\lambda, s, n, d, k) \Big|_{k=0} = \frac{Ax}{B - Cx \cos(\varphi) + Dx^2} \quad (1)$$

$$\text{Here, } A = 16n^2s, \quad B = (n+1)^3(n+s^2), \\ C = 2(n^2-1)(n^2-s^2), \quad D = (n-1)^3(n-s^2) \\ , \varphi = 4\pi nd / \lambda, \quad x = \exp(-\alpha d) \quad \text{and} \quad k = \frac{\alpha\lambda}{4\pi}.$$

All parameters in these equations are a function of wavelength. It is not complex to view that at  $\cos(\varphi) = \pm 1$ , that is, one can reformulate the first equation (Eq. 1) at the extremes of the interference points as follows:

$$T_{Mo} = \frac{Ax}{B - Cx + Dx^2} \quad \text{for (the interference maxima)} \quad (2)$$

And

$$T_{mo} = \frac{Ax}{B + Cx + Dx^2} \quad \text{for (the interference minima)} \quad (3)$$

Schematically, the expression about uniform and non-uniform thin films has been illustrated in Fig. 1 (a & b), respectively. Fig. 1 (b) is presumed that the thickness changes linearly through the illuminated area, thus it can be illustrated by:  $d = \bar{d} \pm \Delta d$ ,  $\Delta d$  refers to the actual changes in thickness from the average thickness  $\bar{d}$ , as appeared in Fig. 1 (b), and must not be confounded with a standard deviation of computed values, RMSE. Deviation utilized by other workers [33]:

$$RMSE = \left( \frac{\sum_{i=1}^q (d - \bar{d})^2}{q} \right)^{0.5} \quad (4)$$

Here,  $q$  is the number of thickness points. The Schematical graph for a film with a wedge-like cross-section is illustrated in Fig. 1 (b). Here, the interference style shrinks dramatically on account of the thickness is not uniform. Now, Eq. (1) must be integrated over both the thickness of the film  $\Delta d$  and  $x$  for it to more exactly depict the

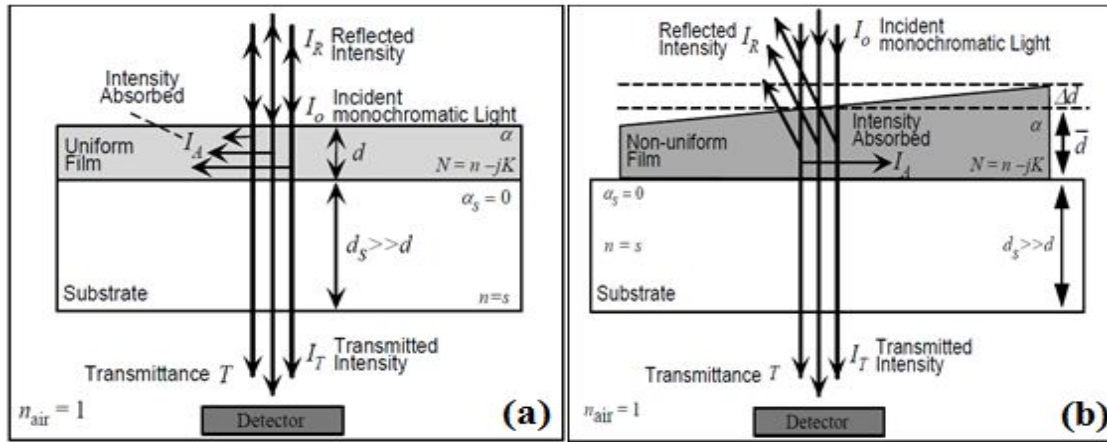


**Fig. 1:** System of an absorbing thin film with a linear variation in (a) uniform (b) non-uniform thickness onto a thick transparent substrate.

transmission spectrum  $T_{\Delta d}(\lambda)$  [8]. The transmittance thus becomes as follows:

$$T_{\Delta d} = \frac{1}{\varphi_2 - \varphi_1} \int_{\varphi_1}^{\varphi_2} \frac{A\bar{x}}{B - C\bar{x} \cos \varphi + D\bar{x}^2} d\varphi \tag{5}$$

Here,  $\varphi_1 = 4\pi n(\bar{d} - \Delta d) / \lambda$ ,  $\varphi_2 = 4\pi n(\bar{d} + \Delta d) / \lambda$  and  $\bar{x} = \exp(-\alpha \bar{d})$ . The integral yields:

$$T_{\Delta d} = \frac{\lambda}{4\pi n \Delta d} \frac{a}{(1-b^2)^{1/2}} \left[ \tan^{-1} \left( \frac{1+b}{(1-b^2)^{1/2}} \tan \frac{\varphi_2}{2} \right) - \tan^{-1} \left( \frac{1+b}{(1-b^2)^{1/2}} \tan \frac{\varphi_1}{2} \right) \right] \tag{6}$$

Here,

$$a = \frac{A\bar{x}}{B + D\bar{x}^2} \quad \text{and} \quad b = \frac{C\bar{x}}{B + D\bar{x}^2} \tag{7}$$

As a result one will have:

Maxima:

$$T_{M\bar{x}} = \frac{\lambda}{4\pi n \Delta d} \frac{a}{(1-b^2)^{1/2}} \left[ \tan^{-1} \left( \frac{1+b}{(1-b^2)^{1/2}} \tan \frac{2\pi n \Delta d}{\lambda} \right) \right] \tag{8}$$

Minima:

$$T_{m\bar{x}} = \frac{\lambda}{4\pi n \Delta d} \frac{a}{(1-b^2)^{1/2}} \left[ \tan^{-1} \left( \frac{1-b}{(1-b^2)^{1/2}} \tan \frac{2\pi n \Delta d}{\lambda} \right) \right] \tag{9}$$

The experimental envelope values  $T_M$  and  $T_m$  for the non-uniform films in terms of the envelope values  $T_{Mo}$  and  $T_{mo}$  in the uniform films, with a thickness equal to the average thickness for non-uniform film, as replacing: Eq. (7) in Eqs. (8 & 9) and utilizing Eq. (5) are written:

$$T_M = \frac{\sqrt{(T_{Mo} T_{mo})}}{\chi} \cdot \tan^{-1} \left[ \sqrt{\left( \frac{T_{Mo}}{T_{mo}} \right)} \cdot \tan \chi \right] \tag{10}$$

$$T_m = \frac{\sqrt{(T_{Mo} T_{mo})}}{\chi} \cdot \tan^{-1} \left[ \sqrt{\left( \frac{T_{mo}}{T_{Mo}} \right)} \cdot \tan \chi \right] \tag{11}$$

Here,

$$\chi = \frac{2\pi n \Delta d}{\lambda} \tag{12}$$

and

$$0 < \chi < \pi/2 \quad (\text{or equivalently, } 0 < \Delta d < \lambda/4n) \tag{13}$$

## 4 Results and Discussion

### 4.1 The Structure Analysis

The stoichiometry of the powder ground from the study alloys is confirmed using EDAX technique. The representative EDAX spectrum of the  $As_{40}Se_{60}$  glassy alloy

exhibited the constituent element ratio is near to the nominal samples as demonstrated in Fig. 2 (as an example).

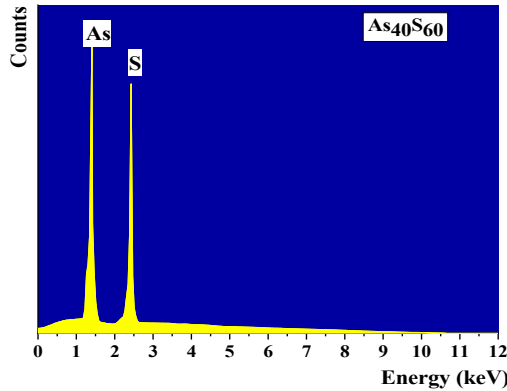


Fig. 2: Energy dispersive X-ray (EDX) spectrum of the As40S60 glassy alloy.

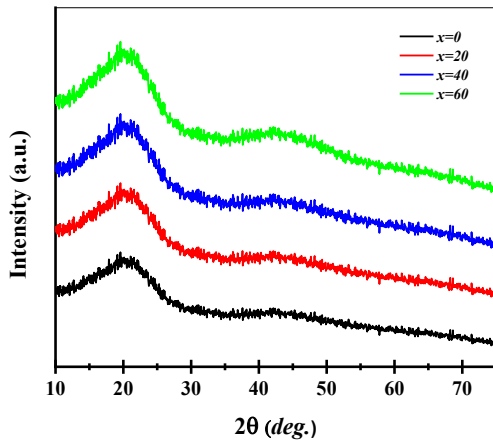


Fig. 3: X-ray patterns of as-prepared studied thin films.

Fig. 3 shows a typical X-ray patterns of the deposited research films. That is, such a graph shows a broad peak without any sharp crystalline peak, indicating the amorphous nature of these films. SEM inspection enhances the amorphous nature of the studied films (see Fig. 4). The SEM images of the studied thin films present homogenous regions free of any type of morphology.

### 4.2 Optical Properties

In a spectral range extended from 400 to 2500 nm, the experimental results illustrated in Fig. 5, the variation of transmission  $T(\lambda)$  and reflection  $R(\lambda)$  spectra of the studied compositions as a function of wavelength. As clearly observed in the transmission spectrum, distinct interference fringes are observed at longer wavelength

(transparent region) with a large intensity approaching  $\approx 86\%$ . As we move to a shorter wavelength where the absorption starts to take place within the film, the intensity of the interference fringes start to decrease gradually until it approached zero at the edge of the optical band-gap of the deposited films. Besides, shrinkage appears in transmission spectra in both weak and medium absorption regions that reflect the non-uniformity of the films.

Firstly, utilizing the Program Origin Version 2018 (OriginLab Corp.), two envelopes,  $T_M$  and  $T_m$  are extracted and drawn around the corresponding extrema points and also are given in Table 1. Secondly, the looker closely in Eqs. (10 & 11) will find that both equations are extremely independent and their solution is not familiar at first sight, as they are outside the limits of experience or more precisely, are transcendental in . In this  $\chi$  and  $T_{mo}$ ,  $T_{Mo}$  case,  $T_{Mo} \equiv T_s$  (here,  $T_s$  is the transmission of the substrate alone) as illustrated in Fig. 6 -for the first studied sample- (as an example) and the  $T_{mo}$  and  $\chi$  have only remained unresolved. Using approximate for the *minerr* nonlinear functions in the Mathcad 2000 program,  $T_{mo}$  and  $\chi$  in equations 10 and 11 are solved. In strong and medium absorption regions, shrinkage of the transmission spectrum of as-deposited As<sub>40</sub>S<sub>60</sub> film is illustrated in Fig. 6.

On the other hand, the fundamental relation for the interference fringe points will be written under previous papers [17, 21, 22] as follows:

$$\frac{l}{2} = \frac{2n\bar{d}}{\lambda} - m_l \quad l = 0, 1, 2, 3, 4, \dots \quad (14)$$

Here:  $m_l$  is the order number at ( $l = 0$ ) extreme considered, an integer for a maximum or half-integer for a minimum. Replacing Eq. (12) in Eq. (14) yields:

$$\frac{l}{2} = \left( \frac{\bar{d}}{\pi\Delta d} \right) \chi - m_l \quad (15)$$

If represented  $\frac{l}{2}$  against  $\chi$  for the transparent region, the

slope, in Eq. (15) can be obtained as  $m$ , and  $\left( \frac{\bar{d}}{\pi\Delta d} \right)$  shown in Fig. 7 (for all studied thin films). Eq. (15) can now be utilized to compute  $\chi$  for the extrema in the

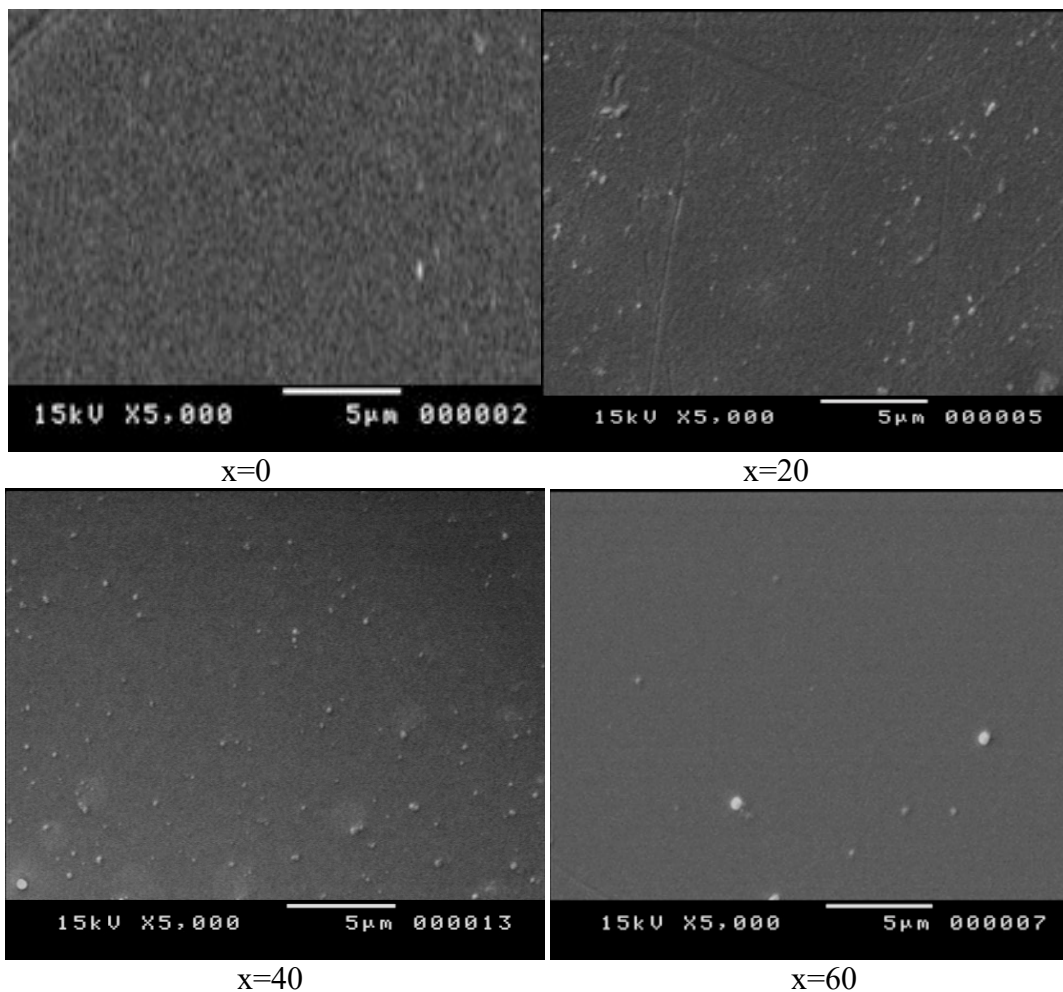


Fig. 4: SEM images showing the surface morphology of the as-prepared studied thin films.

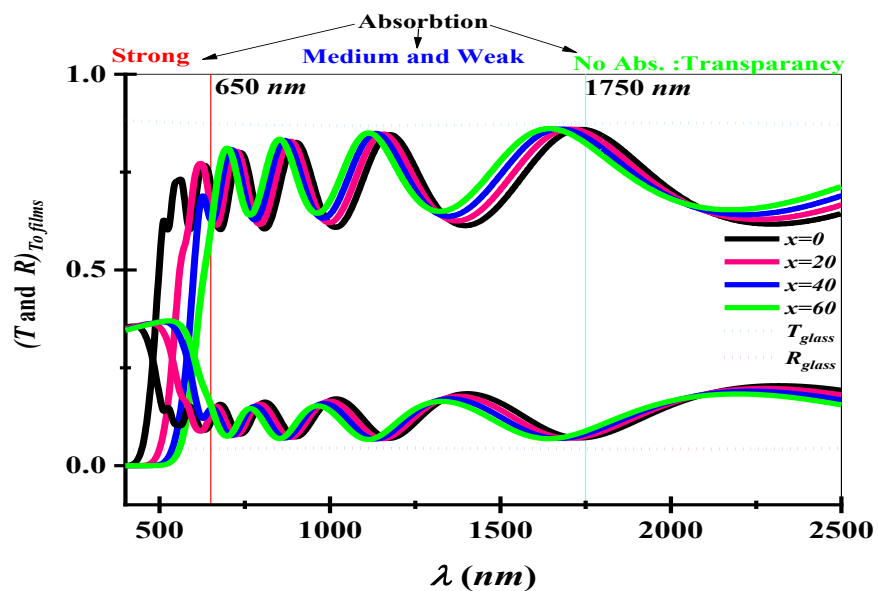
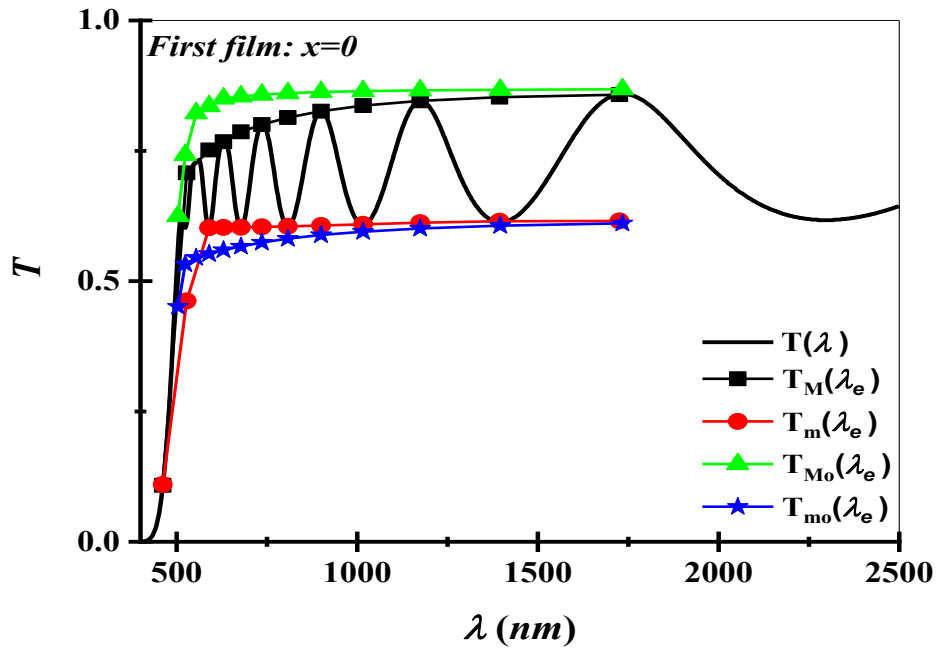
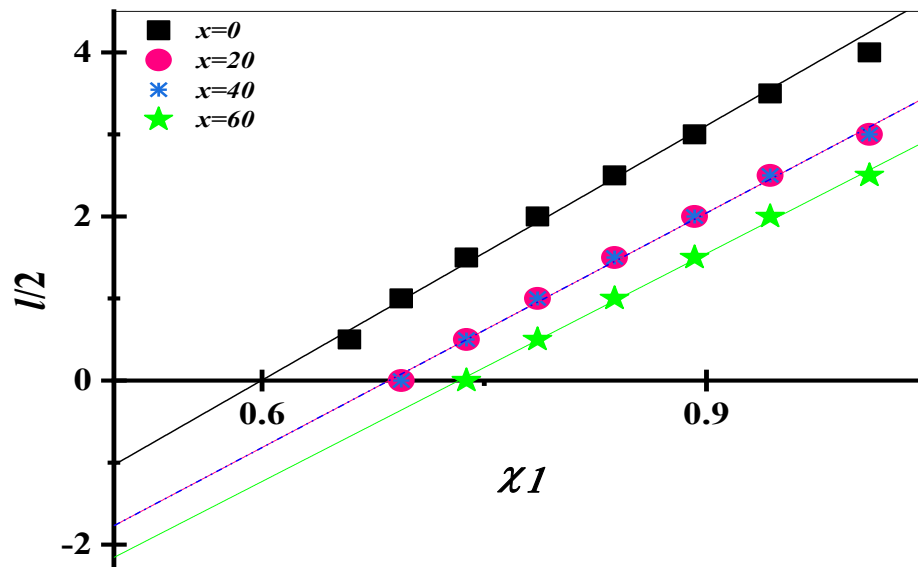


Fig. 5: Transmission and Reflection spectra for the as-prepared thin films.



**Fig. 6:** Shrinkage of transmission spectrum in strong and medium absorption regions of as deposited  $As_{40}S_{60}$  film. The values displayed  $T$  according to the text.



**Fig. 7:** Plot of  $I/2$  against,  $\chi_1$ , in order to determine  $\chi$  for the as-prepared thin films.

absorption region. The new obtained values  $\chi$  are shown  $\chi_1$ , in Table 1. Next, the best straight lines through the points of the transparent region are drawn. The deviation of the points for larger  $\chi$ , from these straight lines indicates the onset of absorption, and these points must be rejected. From Fig. 7 and Eq. (15) can be written the  $(\frac{\bar{d}}{\pi\Delta d}, m_1)$  as (9.90, -5.87), (9.53, -6.53), (9.53, -6.53) and (9.26, -6.78) for all studied films, respectively.

Now, the value of  $\chi$  at each extreme is computed from the values  $(\frac{\bar{d}}{\pi\Delta d}, m_1)$ . The new values  $\chi$ , namely,  $\chi_1$  are shown in Table 1. Using these values of  $\chi_1$ , together with the values of  $T_M$  and  $T_m$ , the  $T_{Mo}$  and  $T_{mo}$  are computed from Eqs. (10 & 11). These values  $T_{Mo}$  and  $T_{mo}$  are shown in Table 1. The obtained values of  $T_{Mo}$  and  $T_{mo}$  can now be utilized to derive:  $\bar{d}$ ,  $\Delta d$  and  $n(\lambda)$  via the method for uniform films discussed in detail in our previous works [21, 22, 30, 31]. The yield values  $\bar{d}$  and  $n(\lambda)$  are summarized in Table. 1.

### 4.3 The Absorption Coefficient, Tauc and Urbach Energy

The absorption coefficient for the studied films has been determined utilizing the following relationship [34, 35]:

$$\alpha(\lambda) = \frac{1}{\bar{d}_2} \times \ln \left[ \frac{(1-R)^2 + \sqrt{\{(1-R)^4 + 4(RT)^2\}}}{2T} \right] \tag{16}$$

Where:  $d$  (cm) is the film thickness. Here,  $\bar{d}_2$  (cm) is the average value of the accurate thickness of thin films, (see Table 1). Fig. 8 reveals the reliance of the absorption coefficient  $\alpha(\lambda)$  on the photon energy ( $h\nu$ ) for the studied samples. One can realize that the increase of Se content in the studied samples enabled us to control the absorption coefficient. This quantity increases with increasing Se content especially in the visible region (400-700 nm) but it shifts toward the lower photon energy as the Se content increases. It is due to an improvement in the concentration of the localized states created by the impurities between the valence and the conduction bonds, in which these values act as a supplementary rate for the transport of electrons obtaining photons with far less energy

than the optical energy gap and afterward the incidence of absorption.

According to Tauc relationship in the strong absorption region ( $\alpha > 10^4 \text{ cm}^{-1}$ ), the energy bandgap for the studied system is determined [36-38]:

$$(\alpha \cdot h\nu) = B \cdot (h\nu - E_g)^r \tag{17}$$

Here:  $B$  is a constant factor that relies on the probability of transformation,  $E_g$  is the energy bandgap of the film, and  $r$  is a number that represents the transformation phase, and has a value of 1/2 for the direct transition and a value of 2 for the indirect transition. Making the substitution that  $Y = \alpha h\nu$ , Eq. (17) can be written in the form [39]:

$$\frac{Y}{Y'} = \frac{1}{r} (h\nu - E_g)$$

Where  $Y$  is the derivative of  $Y$  concerning the photon energy ( $h\nu$ ). Eq. (18) is used to analyze the experimental data since it gives the ratio of  $Y/Y'$  as a linear function of ( $h\nu$ ) and offers a direct method for determining the exponent  $r$ . Fig. 9 displays the dependence of the ratio of  $Y/Y'$  on the photon energy for the studied compositions. The best straight line is drawn through plotted points using the linear regression so the values of  $r$  are  $2 \pm 0.05$ . The value of  $r$  is closed to 2 indicating the electronic transition responsible for the photon absorption is a non-direct process.

Fig. 10 offers the dependence of  $\sqrt{(\alpha \cdot h\nu)}$  on the photon energy, ( $h\nu$ ) for the studied samples. The x-axis intercept indicates the value of the indirect optical band gap,  $E_g$ . The energy band gap values of the studied thin films are determined by extrapolation of the linear regions on the energy axis ( $h\nu$ ) as given in Fig. 10. These values of the optical bandgap of the investigated films are summarized in Table 2. It was found that the optical band gap decrease with increasing Se content. The results are interpreted in terms of the change in concentration of localized states due to the shift in the Fermi level as a result of varying Se content. These optical results confirm that the increasing of Se content increases the effect of scattering on free carriers from ionized impurities. Thin films with a small bandgap have a good potential to absorb ultraviolet rays from electromagnetic radiation by blocking and allowing visible and infrared energy to be transmitted. These values make films perfect and appropriate for solar processing and thermal insulation protective coatings.

**Table 1:-** Values of  $\lambda$ ,  $T_M$  and  $T_m$  for the four different Se content As-S-Se thin films corresponding to transmission spectra. The calculated values of the refractive index and film thickness are based on the wedge shape model.

Sample	$\lambda$	s	$T_M$	$T_m$	$\gamma_1$	$\gamma_2$	$T_{Mo}$	$T_{mo}$	$n_1$	$d_1(nm)$	$m_0$	m	$d_2(nm)$	$n_2$	
As <sub>40</sub> Se <sub>60</sub>	590	1.487	0.7294	0.6024	1.145	1.095	0.8862	0.5523	2.636	0	6.514	6.5	727.4	2.637	
	630	1.466	0.7673	0.603	1.01	1.038	0.893	0.5597	2.596	725.8	6.008	6	728	2.6	
	678	1.452	0.7863	0.6034	0.943	0.98	0.8977	0.5666	2.562	731.4	5.51	5.5	727.7	2.564	
	736	1.442	0.8002	0.6041	0.892	0.922	0.9007	0.574	2.53	726.5	5.012	5	727.3	2.531	
	808	1.434	0.8137	0.6051	0.838	0.865	0.9024	0.5814	2.498	719.2	4.507	4.5	727.9	2.5	
	900	1.429	0.8259	0.6068	0.786	0.807	0.9032	0.5885	2.468	732.0	3.998	4	729.3	2.476	
	1016	1.43	0.8366	0.609	0.738	0.75	0.9034	0.5949	2.447	740.6	3.511	3.5	726.8	2.445	
	1174	1.431	0.8459	0.6121	0.694	0.692	0.9035	0.6009	2.427	730.0	3.014	3	725.6	2.422	
	1396	1.428	0.8529	0.615	0.659	0.635	0.9035	0.6063	2.405	726.2	2.512	2.5	725.5	2.4	
	1734	1.429	0.8578	0.6155	0.632	0.577	0.9035	0.611	2.391	0	2.01	2	725.3	2.385	
$\bar{d}_1 = 728.9625 \text{ nm} \quad \sigma_1 = 5.817 \text{ nm} (0.798 \%) \quad \bar{d}_2 = 727.08 \text{ nm} \quad \sigma_2 = 1.221 \text{ nm} (0.168 \%)$															
As <sub>40</sub> S <sub>20</sub> Se <sub>40</sub>	666	1.454	0.7294	0.6024	1.145	1.095	0.8968	0.5785	2.523	0	5.513	5.5	726.7	2.523	
	722	1.444	0.7673	0.603	1.01	1.038	0.9002	0.5871	2.486	725.1	5.012	5	726.8	2.486	
	794	1.438	0.7863	0.6034	0.943	0.98	0.9021	0.5937	2.461	730.1	4.509	4.5	727.1	2.461	
	882	1.435	0.8002	0.6041	0.892	0.922	0.9031	0.601	2.43	728	4.014	4	725.9	2.43	
	998	1.431	0.8137	0.6051	0.838	0.865	0.9034	0.6079	2.406	725.9	3.508	3.5	726.9	2.406	
	1152	1.428	0.8259	0.6068	0.786	0.807	0.9035	0.6136	2.38	733.7	3.011	3	725.9	2.38	
	1370	1.429	0.8366	0.609	0.738	0.75	0.9035	0.6186	2.359	728.2	2.515	2.5	724.2	2.359	
	1704	1.431	0.8459	0.6121	0.694	0.692	0.9035	0.6231	2.347	0	2.01	2	724.8	2.347	
	$\bar{d}_1 = 728.5 \text{ nm} \quad \sigma_1 = 2.836 \text{ nm} (0.389 \%) \quad \bar{d}_2 = 726.0375 \text{ nm} \quad \sigma_2 = 0.99 \text{ nm} (0.136 \%)$														
	As <sub>40</sub> S <sub>30</sub> Se <sub>30</sub>	656	1.457	0.7294	0.6024	1.145	1.095	0.8959	0.5957	2.478	0	5.525	5.5	733.4	2.478
710		1.446	0.7673	0.603	1.01	1.038	0.8996	0.6021	2.438	771.2	5.046	5	730	2.438	
778		1.439	0.7863	0.6034	0.943	0.98	0.9018	0.6065	2.404	754.1	4.569	4.5	725.5	2.404	
864		1.435	0.8002	0.6041	0.892	0.922	0.9029	0.6138	2.374	711.3	4.069	4	724.2	2.374	
982		1.431	0.8137	0.6051	0.838	0.865	0.9034	0.6219	2.36	709.4	3.534	3.5	729.6	2.36	
1134		1.428	0.8259	0.6068	0.786	0.807	0.9035	0.6278	2.336	739	3.031	3	729.2	2.336	
1346		1.429	0.8366	0.609	0.738	0.75	0.9035	0.6327	2.311	734.9	2.537	2.5	726	2.311	
1676		1.431	0.8459	0.6121	0.694	0.692	0.9035	0.6363	2.302	0	2.028	2	726.5	2.302	
$\bar{d}_1 = 736.65 \text{ nm} \quad \sigma_1 = 21.954 \text{ nm} (2.98 \%) \quad \bar{d}_2 = 728.0 \text{ nm} \quad \sigma_2 = 2.83 \text{ nm} (0.389 \%)$															
As <sub>40</sub> Se <sub>60</sub>		766	1.44	0.7294	0.6024	1.145	1.095	0.9016	0.6192	2.375	0	4.5	4.5	727.3	2.375
	852	1.436	0.7673	0.603	1.01	1.038	0.9028	0.6275	2.349	735.6	3.995	4	728.2	2.349	
	962	1.434	0.7863	0.6034	0.943	0.98	0.9033	0.6326	2.32	743.4	3.512	3.5	724.9	2.32	
	1112	1.434	0.8002	0.6041	0.892	0.922	0.9035	0.6374	2.299	741.6	3.017	3	723.3	2.299	
	1316	1.431	0.8137	0.6051	0.838	0.865	0.9035	0.6416	2.267	707.7	2.531	2.5	718.5	2.288	
	1660	1.428	0.8259	0.6068	0.786	0.807	0.9035	0.6468	2.288	708.2	1.989	2	731.3	2.267	
	2184	1.429	0.8366	0.609	0.738	0.75	0.9035	0.6509	2.258	0	1.504	1.5	725.4	2.258	
	$\bar{d}_1 = 727.3 \text{ nm} \quad \sigma_1 = 16.01 \text{ nm} (2.201 \%) \quad \bar{d}_2 = 725.5571 \text{ nm} \quad \sigma_2 = 3.748 \text{ nm} (0.517 \%)$														

For the absorption coefficient ( $\alpha$ ) of less than  $10^4 \text{ cm}^{-1}$ , namely, ( $10^{-1} < \alpha < 10^4$ )  $\text{cm}^{-1}$ , the exponential edge region, there is usually Urbach tail, where ( $\alpha$ ) increases exponentially with the photon energy ( $h\nu$ ) according to Urbach's empirical relation, we utilized Pankove's expression [40]:

$$\alpha(h\nu) = \alpha_0 \exp\left(\frac{h\nu}{E_e}\right) \tag{19}$$

Where:  $\nu$  is the frequency of the radiation  $M$  is a constant,  $E_e$  is interpreted as the width of the tails of

localized states in the gap region and, in general, represents the degree of disorder in an amorphous semiconductor and  $\alpha_0$  represents a constant. Therefore, plotting the reliance of  $\ln(\alpha)$  on  $h\nu$  gives a straight line as offered in Fig. 11. The inverse of the yield slope gives the band tail width,  $E_e$  of the localized states. The effects of an increase of Se content on  $E_g$  and  $E_e$  are summarized in Table. 2. It is observed from this table that the band tail width  $E_e$  increased with increasing Se content and the optical energy gap  $E_g$  changes in an exactly opposite manner. The increase in value of  $E_e$  with the increasing Se content may also be

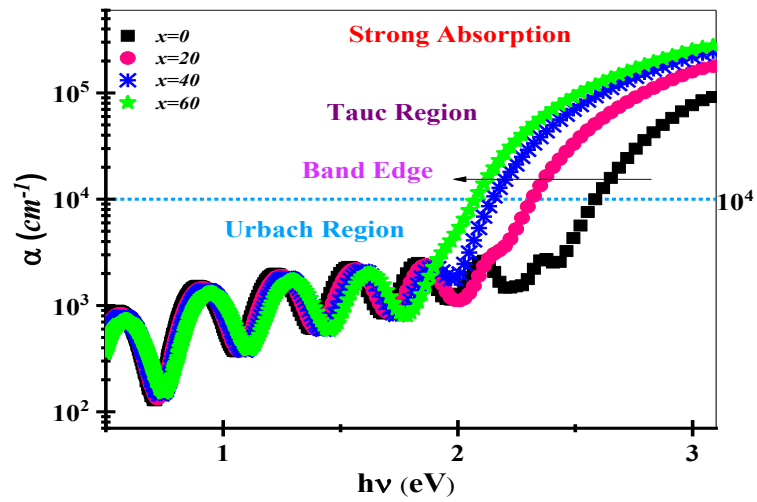


Fig. 8: Plotting of absorption coefficient for the studied thin films as a function of photon energy.

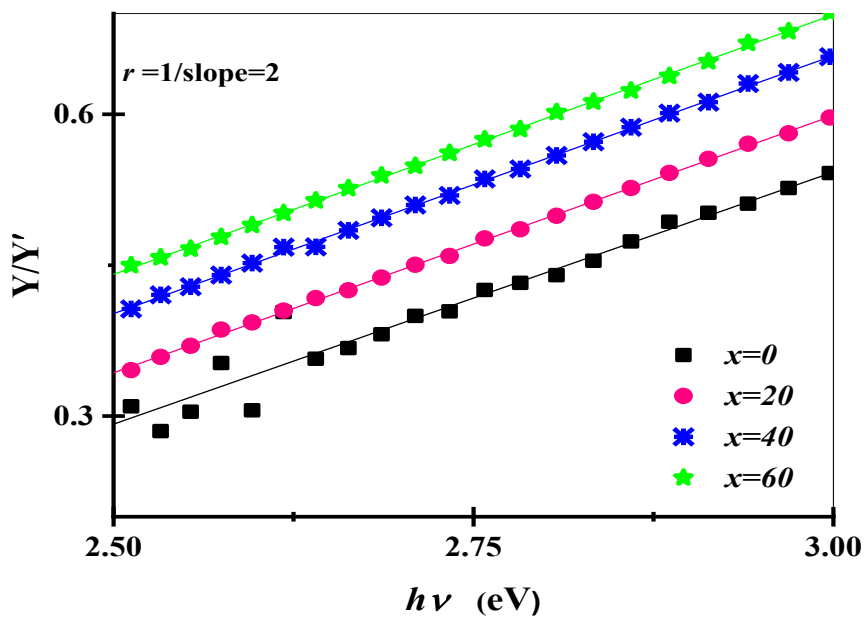


Fig. 9: The dependence of the ratio of  $Y/Y'$  on the photon energy for the studied thin films.

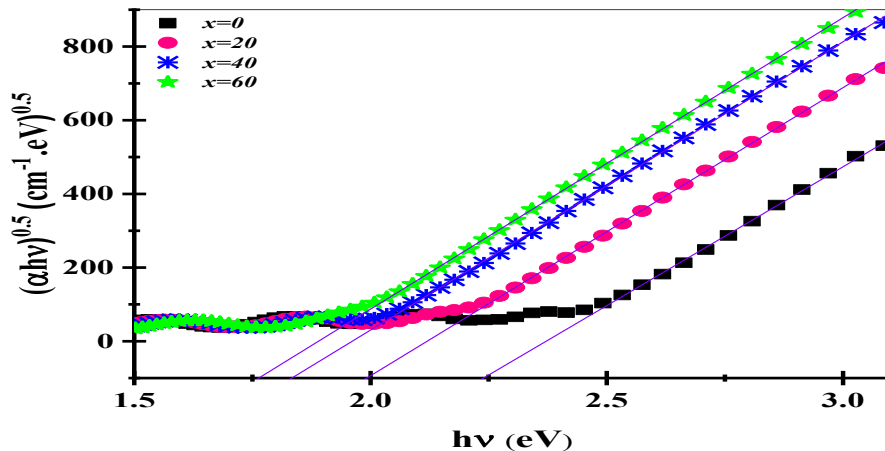


Fig. 10: The plot of  $(\alpha \cdot hv)^{0.5}$  versus photon energy,  $(hv)$  for the studied thin films.

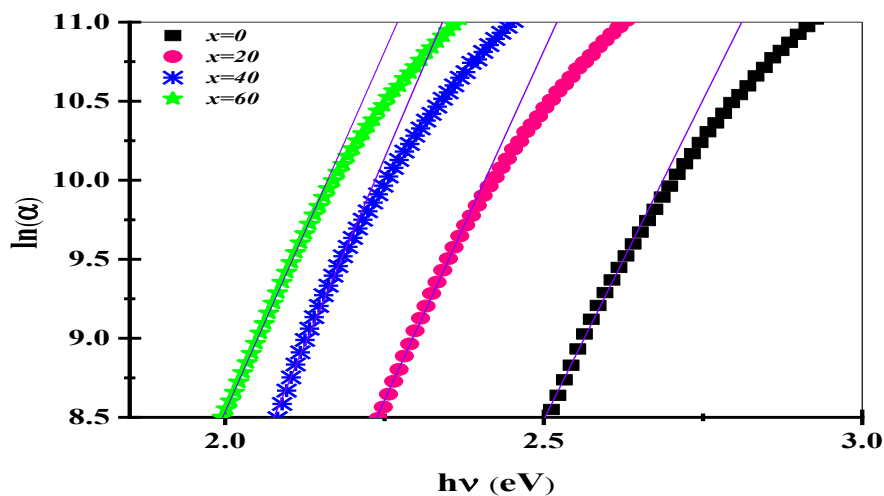


Fig. 11: The plot of  $\ln(\alpha)$  versus photon energy,  $(hv)$  for the studied thin films.

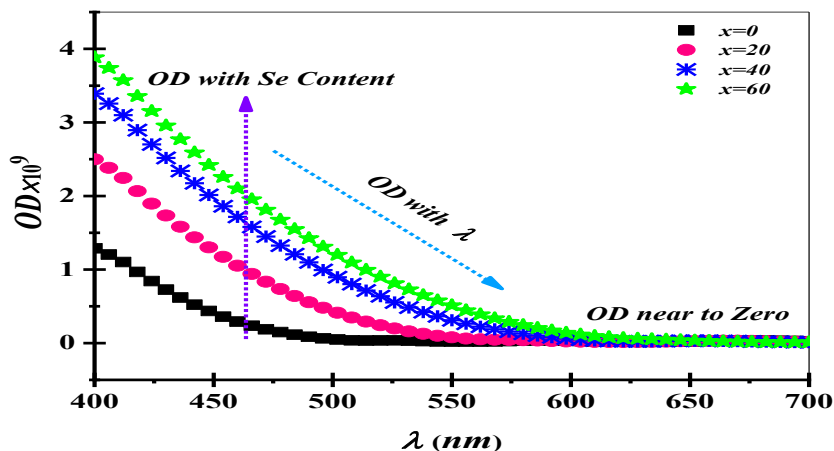


Fig. 12: The dependence of optical density,  $OD$  on Se content and wavelength  $(\lambda)$  for the studied thin films

**Table 2:** Optical and electrical parameters for the studied thin films. The meanings of the parameter codes as stated in the text.

$x$	$E_g$ (eV)	$E_e$ (eV)	$E_o$ (eV)	$E_d$ (eV)	$n(o)$
0	2.38	0.159	4.34	19.88	2.36
20	2.13	0.172	4.37	19.19	2.32
40	1.97	0.186	4.40	18.32	2.27
60	1.90	0.190	4.50	18.14	2.24

attributed to the increase in the film structural disorders. Here it should be noted that  $E_g$  and  $E_e$  are called the linear optical parameters.

Regarding connection, we must explain an important optical concept, namely optical density. Optical density is defined as the process by which matter transmits light or other electromagnetic radiation. Both the emission and absorption processes are based on the wavelength of radiation, including the interaction between electrons, atoms, ions and other elementary particles. When the beam interacts with absorbing atoms, absorption occurs. It is based on the thickness of the sample and the concentration of absorbed atoms and particles. Since the optical density is the ratio of the absorption coefficient,  $\alpha$  [35] to the thickness of the film, one can write the optical density  $d$  as follows:

$$OD = \frac{\alpha}{d} \quad (20)$$

Fig. 12 represents the plots of optical density ( $OD$ ) against the wavelength ( $\lambda$ ) according to Eq. 20. The results refer to a reduction of the optical density with increasing wavelength and it increases with increasing Se content. As we all know, optical density is a measure of the ability of refractive media or optical components to slow down or delay light transmission. That is, it measures the speed of light passing through the material affected by the wavelength of the light wave. The higher the frequency at which light can travel through a given medium, the slower the optical density of the medium, and vice versa; absorbance measures the ability of a refractive medium or optical component to absorb light. Namely, absorbance measures how much light is lost when light passes through a given medium. On the other side, in the absence of absorption, the optical density also considers the scattering or refraction of light.

#### 4.4 Linear Optical Constants

Linear optical constants are the expressions used only to define the refractive index,  $n$ , and the absorption index (the extinction coefficient),  $k_{ex}$  of the studied compositions.

The refractive index,  $n(\lambda)$  of the analyzed compositions across the entire spectrum (400-2500 nm) has been determined from the following formula [41]:

$$n(\lambda) = \left[ a + \frac{b}{\lambda^2} \right] \quad (21)$$

Where,  $a$  and  $b$  are Cauchy's constants.

According to Eq. (21), Fig. 13 highlights the reliability of the refractive index of the analyzed thin films on the wavelength of the photon. The decrease of the refractive index by increasing the wavelength is called the normal dissipation (as in our current work), and this dissipation is anomalous if the refractive index increases with increasing wavelength. On the other hand, it is evident from Fig. 13 that the evidence for the refraction of thin films is increased by increasing the content of Se (this behavior was observed in other works [42, 43]).

On the other corner, the spectral variation of the calculated absorption index (the extinction coefficient,  $k_{ex}$ ) against the wavelength of the investigated samples is illustrated in Fig. 14 according to the following formula [44]:

$$k_{ex} = \frac{1}{4\pi} (\alpha \cdot \lambda) \quad (22)$$

The scattering of light and the decrease of absorption are significant factors for the reduction of absorption coefficients in a relatively high absorption area, with their total absence in the rest of the absorption regions and transparency. It serves to ensure that the light rays do not dissipate and lose in these areas, as opposed to the strong absorption region. In general, the optical constants,  $n$  and

$k_{ex}$  increase with increasing Se content in the studied system.

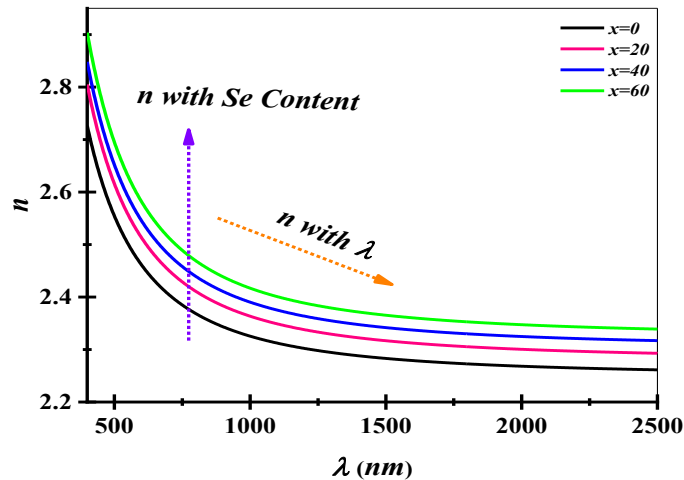


Fig. 13: The dependence of refractive index on Se content and wavelength ( $\lambda$ ) for the studied thin films.

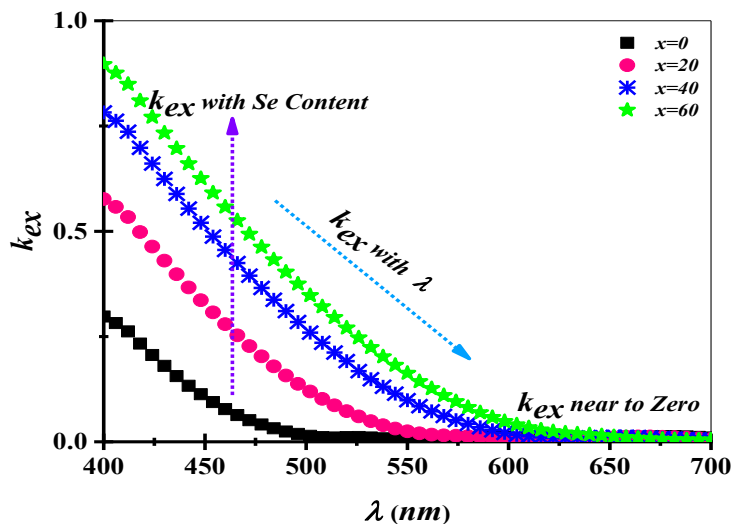


Fig. 14: The dependence of extinction coefficient on Se content and wavelength ( $\lambda$ ) for the studied thin films.

## 5 Conclusions

The current work displays the wedge-shaped method for as-obtained As-Se-S thin films utilizing only the transmission spectrum at normal incidence via a UV/Vis/NIR

pectrophotometer. In this framework, the procedures are utilized to compute the average thickness from wedge-shaped behavior. The increase of Se concentration that ranged between 0 and 60 is lead to improving the regularity of the thickness of the studied thin films and accordingly, the possibility of asserting that such thin films according to this procedure that we covered in our work is a promising future will be served a modern technology.

## Conflict of Interest

All authors declare that there is no conflict of interest regarding the publication of this paper.

## Reference

- [1] Solis, J., Afonso, C. N., Hyde, S. C. W., Barry, N. P., & French, P. M. W. PRL., **76**, 2519 (1996).
- [2] Coombs, J. H., Jongenelis, A. P. J. M., van Es-Spiekman, W., & Jacobs, B. A. J. Appl 78 4906-4917 (1995).
- [3] Hilton, A. R. J Non Cryst Solids., **2**, 28-39 (1970).
- [4] Singh, Abhay Kumar. Cryst. Res. Technol. 29-64 (2012).

- [5] Frerichs, Rudolf. *JOSA.*, **43**, 1153-1157 (1953).
- [6] E. R. Shaaban, *Physica B: condensed matter.* **373** (2), 211-216 (2006).
- [7] Swanepoel, R. *J Phys E Sci Instrum.*, **16**, 1214 (1983).
- [8] Swanepoel, R. *J Phys E Sci Instrum.* **17** 896 (1984).
- [9] Gonzalez-Leal, J. M., Prieto-Alcon, R., Stuchlik, M., Vlcek, M., Elliott, S. R., & Marquez, E. *Opt. Mater.*, **27**, 147-154 (2004).
- [10] Štrbac, D. D., Lukić, S. R., Petrović, D. M., Gonzalez-Leal, J. M., & Srinivasan, A. *J Non Cryst Solids.*, **353**, 1466-1469 (2007).
- [11] Shaaban, E. R., El-Kabnay, N., Abou-Sehly, A. M., & Afify, N. *Physica B Condens.*, **381** 24-29, (2006).
- [12] Ruiz-Pérez, J. J., González-Leal, J. M., Minkov, D. A., & Márquez, E. *J. Phys. D: Appl. Phys.*, **34**, 2489 (2001).
- [13] Shaaban, E. R. *Philos. Mag.*, **88**, 781-794 (2008).
- [14] Cardinal, T., Richardson, K. A., Shim, H., Schulte, A., Beatty, R., Le Foulgoc, K., ... & Villeneuve, A. *J Non Cryst Solids.*, **256**, 353-360 (1999).
- [15] Sanghera, Jas S., Vinh Q. Nguyen, and Ishwar D. Aggarwal. *J. Am. Ceram. Soc.*, **79**, 1324-1328 (1996).
- [16] E. R. Shaaban, M. S. Abd El-Sadek, M.El-Hagary, I. S.Yahia, *Physica Scripta* **86** (1), 015702 (2012)
- [17] MÁrquez, S. E., Ramirez-Malo, J., Villares, P., Jimenez-Garay, R., Ewen, P. J. S., & Owen, A. E. *J. Phys. D: Appl. Phys.*, **25**, 535 (1992).
- [18] Cimpl, Z., and F. Kosek *Phys. Status Solidi A* **93** K55-K58 (1986).
- [19] Minkov, D., et al. (1987). *Journal of Non-Crystalline Solids* ., **90(1-3)**, 481-484.
- [20] Manificier, J. C., J. Gasiot, and J. P. Fillard. *J Phys E Sci Instrum.*, **9**, 1002 (1976).
- [21] Shaaban, E. R. *Mater. Chem. Phys.* **100**. 411-417 (2006).
- [22] Shaaban, E. R., M. Abdel-Rahman, and M. T. Dessouky. *Thin Solid Films.*, **515**, 3810-3815 (2007).
- [23] Manificier, J. C., J. Gasiot, and J. P. Fillard. *J Phys E Sci Instrum.*, **9**, 1002 (1976).
- [24] Gonzalez-Leal, J. M., Prieto-Alcon, R., Stuchlik, M., Vlcek, M., Elliott, S. R., & Marquez, E. *Opt. Mater.*, **27**,147-154 (2004).
- [25] Štrbac, D. D., Lukić, S. R., Petrović, D. M., Gonzalez-Leal, J. M., & Srinivasan, A. *J Non Cryst Solids.*, **353**, 1466-1469 (2007).
- [26] Ruiz-Pérez, J. J., González-Leal, J. M., Minkov, D. A., & Márquez, E. *J. Phys. D: Appl. Phys.*, **34**, 2489 (2001).
- [27] Marquez, E., Bernal-Oliva, A. M., Gonzalez-Leal, J. M., Prieto-Alcon, R., Ledesma, A., Jimenez-Garay, R., & Martil, I. *Mater. Chem. Phys.*, **60**, 231-239 (1999).
- [28] Cardinal, T., Richardson, K. A., Shim, H., Schulte, A., Beatty, R., Le Foulgoc, K., ... & Villeneuve, A. *J Non Cryst Solids.*, **256**, 353-360 (1999).
- [29] Sanghera, Jas S., Vinh Q. Nguyen, and Ishwar D. Aggarwal. *J. Am. Ceram. Soc.*, **79**, 1324-1328 (1996).
- [30] Shaaban, E. R., Hassaan, M. Y., Moustafa, M. G., Qasem, A., & Ali, G. A. *Optik.*, **186** ,275-287 (2019).
- [31] Shaaban, E. R., Hassaan, M. Y., Moustafa, M. G., Qasem, A., Ali, G. A. M., & Yousef, E. S. *Acta Phys. Pol.*, **136**, (2019).
- [32] Shaaban, E. R., Hassaan, M. Y., Moustafa, M. G., & Qasem, A. *Appl. Phys. A* **126** 34 (2020).
- [33] Pal, U., Saha, S., Chaudhuri, A. K., Rao, V. V., & Banerjee, H. D. *J. Phys. D: Appl. Phys.*, **22**, 965 (1989).
- [34] Pankove, Jacques I., 1975.
- [35] Shaaban, Essam R., N. Afify, and Atef El-Taher. *J. Alloys Compd.*, **482**, 400-404 (2009).
- [36] Enderby, J. E., and A. C. Barnes. (1974).
- [37] Tauc, J., Radu Grigorovici, and Anina Vancu. *Phys. Status Solidi B.*, **15**, 627-637 (1966).
- [38] Davis, E. A., and Nff Mott. *Philos. Mag.*, **22**, 0903-0922 (1970).
- [39] Ray, A. K., and C. A. Hogarth. *J. Phys. D: Appl. Phys.* **23** 458 (1990).
- [40] E. R. Shaaban, Y. A. M. Ismail, H. S. Hassam, *Journal Non-crystalline solids.*, 376, 61-67 (3013).
- [41] Aparimita, A., Sripan, C., Ganesan, R., Jena, S., & Naik, R. *Phase Transit.* **91** 872-886 (2018) .
- [42] Gonzalez-Leal, J. M., Prieto-Alcon, R., Angel, J. A., & Marquez, E. *J Non Cryst Solids.*, **315**, 134-143 (2003).
- [43] M. Emam-Ismail.M. El-Hagary, E. R. Shaaban, A. M. Al Hedeib, *Journal of Alloys and Compounds* **532**, 16-24 (2012)
- [44] Shokr, E. Kh, and M. M. Wakkad. *J. Mater. Sci.*, **27**, 1197-1201 (1992).